CHINESE OPTICS LETTERS

Vol. 21, No. 5 | May 2023

Hundred-watt level all-fiber visible supercontinuum generation from a graded-index multimode fiber

Li Jiang (江 丽)[1,2], Rui Song (宋 锐)[1,2,3*], and Jing Hou (侯 静)[1,2**]

[1] College of Advanced Interdisciplinary Studies, National University of Defense Technology, Changsha 410073, China

[2] Nanhu Laser Laboratory, National University of Defense Technology, Changsha 410073, China

[3] Key Laboratory of Atmospheric Optics, Anhui Institute of Optics and Fine Mechanics, Chinese Academy of Sciences, Hefei 230031, China

*Corresponding author: srnotice@163.com

**Corresponding author: houjing25@sina.com

Received November 20, 2022 | Accepted March 10, 2023 | Posted Online April 17, 2023

A monolithic visible supercontinuum (SC) source with a record average output power of 204 W and a spectrum ranging from 580 nm to beyond 2400 nm is achieved in a piece of standard telecom graded-index multimode fiber (GRIN MMF) by designing the pumping system. The influence of the GRIN MMF length on the geometrical parameter instability (GPI) effect is analyzed for the first time, to the best of our knowledge, by comparing the SC spectral region dominated by the GPI effect under different fiber lengths. Our work could pave the way for robust, cost-effective, and high-power visible SC sources.

Keywords: visible supercontinuum; high-power supercontinuum; graded-index multimode fiber; geometrical parameter instability; nonlinear optics.

DOI: 10.3788/COL202321.051403

1. Introduction

Visible supercontinuum (SC) has been a hot research topic in recent years due to its application in hyperspectral light detecting and ranging (LiDAR), broadband illumination, and display technologies[1,2]. The traditional method used for visible SC generation uses a pulsed laser to pump a piece of photonic crystal fiber (PCF), in which the PCF with capability of controlling dispersion enables visible SC output[3–5]. Typically, the core size of the PCF is designed to be small enough to ensure an effective short wavelength extension of the SC. However, this limits its high-power handling capacity[6–8].

Multimode fiber (MMF) is promoted as having high-power handling potential. In comparison with the step-index MMF, the graded-index multimode fiber (GRIN MMF) has attracted much attention due to its unique properties. First, the GRIN MMF has a lower Kerr self-cleaning threshold because its periodic index gratings caused by strong periodic oscillation will convert more energy from the higher-order modes to the fundamental mode[9–11]. In terms of SC generation, the combined action of the Kerr effect and the Raman effect achieves a bell-shaped beam output in the GRIN MMF[12]. Second, for a quasi-continuous pump pulse propagating in the normal dispersion regime, the nonlinear index grating will lead to a series of intense quasi-phase-matched four-wave mixing, or geometrical parameter instability (GPI), sidebands in the visible and near-infrared regions[13]. Their characteristics enable a high brightness visible SC generation from a GRIN MMF.

SC generation from a GRIN MMF was first demonstrated experimentally in 2013[14]. In 2015, ultra-short pulses were launched in the anomalous dispersion regime (1550 nm) of the GRIN MMF, and a series of peaks with unequal spacing were observed in the visible region, which is attributed to the interplay between spatiotemporal soliton oscillations and dispersive waves (DWs)[15]. Subsequently, in 2016, a flat, broadband SC ranging from 450 nm to 2500 nm was reported in a low differential group delay GRIN MMF when pumping in a normal dispersion regime (1064 nm), in which the new mechanism of the GPI effect enables efficient visible SC generation[16]. Previous studies had simulated the relationship between the GPI effect and the GRIN MMF length on a shorter fiber scale (< 1 m). The results indicated that the GPI first generates a series of narrow spectral sidebands, which subsequently broaden upon propagation[13]. However, the influence of the GRIN MMF length on the GPI effect on a longer fiber scale is difficult to demonstrate numerically and experimentally because other nonlinear effects relating to fiber length will affect the experimental results. In addition, the effective shortwave extension of the SC driven by the GPI effect in the GRIN MMF requires a high pump peak power. Based on this reason, the maximum average output power of the SC generation from the GRIN MMF with an

all-fiber structure is only maintained at about 2 W, as reported in 2022, and the corresponding spectrum covers the wavelength from 450 nm to beyond 2400 nm[17].

In this paper, we explore the potential for all-fiber visible SC power scaling based on a standard telecom GRIN MMF and analyze the influence of the GRIN MMF length on the GPI effect. In the pump system of the three-stage master oscillator power amplifier (MOPA) configuration, a 40 W SC source with a spectrum ranging from 450 nm to beyond 2400 nm is obtained using a piece of highly doped gain fiber with a larger core size of 30/250 μm in the Amplifier 2. To further improve the output power of the SC, a four-stage MOPA configuration is employed, in which the shorter gain fiber length of the Amplifier 3 is selected, and the different pulse durations of seed laser are compared. The output power of the SC is boosted to 204 W, and the corresponding spectrum ranges from 580 nm to beyond 2400 nm. In addition, the influence of the GRIN MMF length on the GPI effect is demonstrated by comparing the spectra of the SC under different GRIN MMF lengths in the spectral region dominated by the GPI effect.

2. SC Power Scaling Based on a GRIN MMF

2.1. 40 W broadband SC generation based on a three-stage MOPA configuration

The experimental setup for a high-power broadband SC generation from a GRIN MMF is shown in Fig. 1, where an ytterbium-doped three-stage MOPA configuration is employed. The pump laser used as the pump of the GRIN MMF consists of a pulsed seed laser and a two-stage amplifier. The 1064 nm pulsed seed laser with tunable repetition rates and pulse durations is employed here. In Amplifier 1, a 27 W 976 nm laser diode (LD) works as the pump and a $(2+1)\times 1$ fiber combiner is used for coupling the pump and the seed laser into a piece of 10/125 μm ytterbium-doped double-clad fiber (YDF). In order to prevent the excessive spectral broadening in Amplifier 2, the output power of Amplifier 1 is controlled at about 2 W. Finally, in Amplifier 2, two 90 W 976 nm LDs are used to provide the pump, and a piece of 30/250 μm YDF with a fiber length of 1 m is used as the gain media. The large-mode-field area YDF with a high absorption coefficient of ∼20 dB/m at 976 nm is used to reduce the spectral broadening of Amplifier 2. These experimental settings used to reduce the spectral broadening of Amplifier 2 aim at increasing the injected pump peak power of the GRIN MMF when boosting the pump average power. A low differential modal group delay GRIN MMF with a core diameter of 50 μm (YOFC, OM4) is used as the nonlinear medium for the visible SC generation. A piece of 30/120 μm germanium-doped fiber (GDF) is used as the transition fiber and is applied between the 30/250 μm YDF and the 50/125 μm GRIN MMF to achieve a low-loss and all-fiber structure. The output fiber pigtail of the GRIN MMF is angle cleaved by 8° to avoid optical feedback.

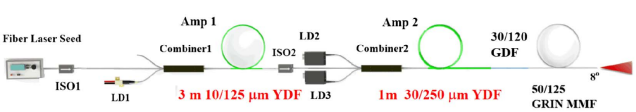

Fig. 1. Experimental scheme for high-power broadband SC generation. ISO, isolator; LD, laser diode; Amp, amplifier.

The output power of the SC was detected by two wavelength insensitive thermal power meters (Ophir, FL250A-BB-50-PPS; Laserpoint, A-600-D60-SHC). The output spectrum was collected by a multimode fiber and recorded by two optical spectrum analyzers (Yokogawa, AQ6374 and AQ6375) with spectral bands of 350–1750 nm and 1200–2400 nm, respectively. To eliminate the multi-order diffraction during the measurement process, a long wavelength-pass filter was used. The measured spectra were spliced together according to aligning spectral intensity.

The seed laser delivers a pulse duration of 1 ns at a repetition rate of 0.5 MHz first. The spectrum and power evolution of the pump laser (i.e., measuring the output spectrum and power of Amplifier 2) with increasing LD power are shown in Fig. 2. A piece of GRIN MMF with a fiber length of 0.5 m and an angle cleaved by 9° is fused to the output fiber of Amplifier 2 and acts as the end-cap output. As seen in Fig. 2(a), the stimulated Raman scattering dominates the initial spectrum broadening, and the first-order Raman peaks located at the wavelength of 1120 nm have appeared in the spectra. With increasing LD power, the long wavelength edge of the spectrum is extended to the anomalous dispersion regime of the fiber (∼1300 nm). The modulation instability starts to play a leading role and makes the nanosecond signal pulses split into a train of ultrashort pulses. Then soliton-related effects, such as soliton self-frequency shift and soliton fission, push the long wavelength edge of the spectrum up to 2 m. Figure 2(b) shows that the conversion efficiency of the LD power to the pump laser is ∼59%.

The SC spectral evolution with increasing pump laser power at 10 m GRIN MMF is plotted in Fig. 3. In order to clearly observe the mechanisms influencing the SC spectral evolution, the x-coordinate is converted from the wavelength to the frequency. With the pump power increasing, apart from the stimulated Raman scattering (SRS) frequency peaks located at 14 THz and 27 THz, some sharp frequency peaks appear between 100 THz and 400 THz. The peaks are typical features of the GPI effect, which is caused by the collective oscillations

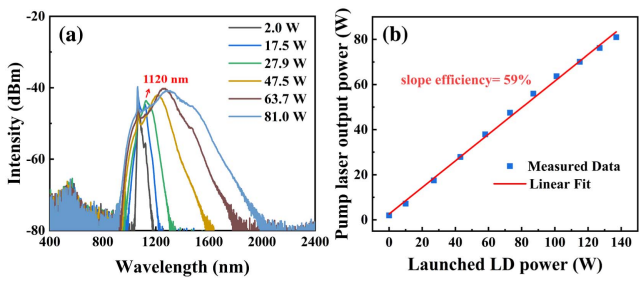

Fig. 2. (a) Spectrum and (b) power evolution of the pump laser with increasing LD power.

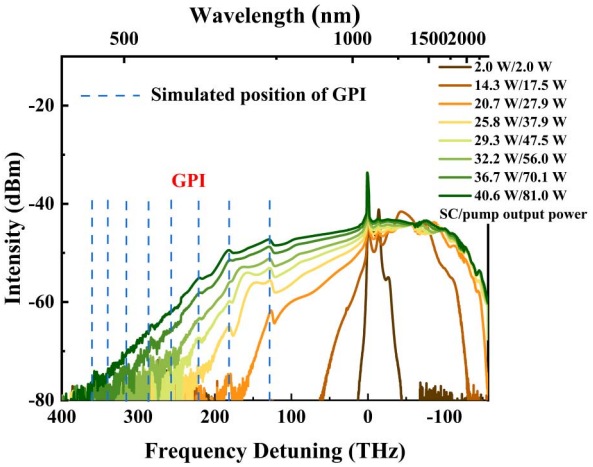

Fig. 3. Measured spectral evolution of the SC with increasing pump laser power at 10 m GRIN MMF. The legend represents the SC output power versus the pump laser output power.

occurring in the GRIN MMF[13]. The corresponding frequency positions of the generated mth GPI sidebands can be obtained by the equation $f_m \approx \pm\sqrt{h} f_1$, where $2\pi f_1 = \sqrt{2\pi/(\xi k'')}$, and h is an integer, $h = 1, 2, 3 \ldots$. Here, κ'' is the fiber dispersion at the pump wavelength, and ξ is the self-imaging period. The measured value of f_1 is about 128 THz, and the other frequency positions are in good agreement with the simulated ones. Such large frequency shifts will combine with other nonlinear effects, such as soliton-related effects[18–20] and stimulated Raman scattering[14,21,22], to link the visible and near-infrared domain, forming a flat continuum.

Figure 4(a) depicts the final spectrum of the SC under the maximum SC output power of 40.6 W. The achieved spectrum of the SC covers the wavelength from 450 nm to beyond 2400 nm, which corresponds to the pump peak power of about 162 kW. The inset of Fig. 4(a) shows the near-field beam profiles of the total and filtered SC at different central wavelengths of 730 nm, 620 nm, 532 nm, and 470 nm, respectively. The SC was sliced by a set of filters with 10 nm bandwidth. The near-field beam profile deteriorates slightly as the wavelength decreases,

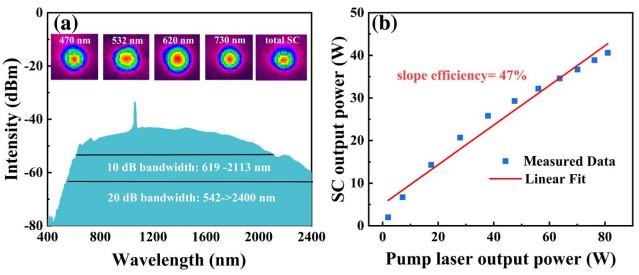

Fig. 4. (a) The final spectrum of the SC at 10 m GRIN MMF with an average SC output power of 40.6 W. The inset shows the near-field beam profiles of the total and filtered SC at different central wavelengths of 730 nm, 620 nm, 532 nm, and 470 nm measured at maximum SC output power. (b) The SC output power versus the pump laser output power.

and resulting from that, more high-order modes are excited in the GRIN MMF at the shorter wavelength[23]. Overall, these differences of beam profile are not great because the Kerr self-cleaning effect existing in the GRIN MMF will shorten these differences by converting more energy from the high-order modes to the fundamental modes[9–11]. Figure 4(b) plots the SC output power varying with the pump laser power, and the results show that the conversion efficiency of the pump laser to SC is about 47%.

2.2. Hundred-watt level SC generation based on a four-stage MOPA configuration

In order to explore the potential for SC power scaling, we add a fiber amplifier following the 30/250 μm YDF of Fig. 2. The experimental scheme is shown in Fig. 5. It is different from the experimental setup of Fig. 2 in that the output powers of Amplifier 1 and Amplifier 2 are controlled at about 10 W and 20 W, respectively. In Amplifier 3, a $(6 + 1) \times 1$ fiber combiner is used for coupling the pump laser from two 800 W 976 nm pump models to a piece of 30/600 μm YDF. Each pump model consists of seven 130 W 976 nm LDs. The 30/600 μm YDF with an absorption coefficient of 1.4 dB/m at 976 nm and an optimized fiber length of 9 m is used as the gain medium and is used to reduce the spectral broadening of Amplifier 3. In order to ensure excellent beam quality and effective heat management, the 30/600 μm YDF is coiled and fixed in the water-cooled plate with a figure-of-eight fiber groove. A homemade 30/600–50/125 mode field adaptor (MFA) is applied in between to bridge the fiber. A piece of the GRIN MMF with a fiber length of 10 m is used for SC generation. An endcap with an angle cleaved by 8° is used to avoid optical feedback.

Hereafter, the pulse duration of the seed laser is optimized to improve the output performance of the SC. Figure 6 shows the dependence of the SC output characteristics on the pulse duration of the seed laser. The repetition frequency of the seed laser is maintained at 2 MHz. The three kinds of different pulse durations (1 ns, 3 ns, and 6 ns) are employed here. The pump power of the system with the pulse duration of 3 ns and 1 ns cannot reach the same pump power as 6 ns, which is caused by the thermal load that exists in the MFA located between 30/600 μm YDF and 50/125 μm GRIN MMF. This thermal load is caused by the loss of light outside the operating wavelength of the MFA, that is, the wider the spectrum broadening in the preceding stage induced by the shorter pulse duration, the more serious the

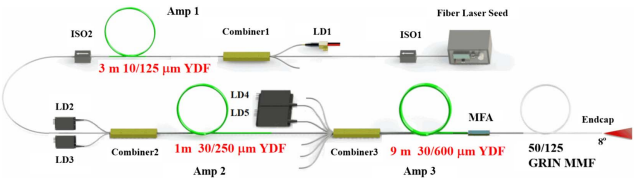

Fig. 5. The experimental scheme for the hundred-watt level SC generation from a GRIN MMF. ISO, isolator; LD, laser diode; Amp, amplifier; MFA, mode field adapter.

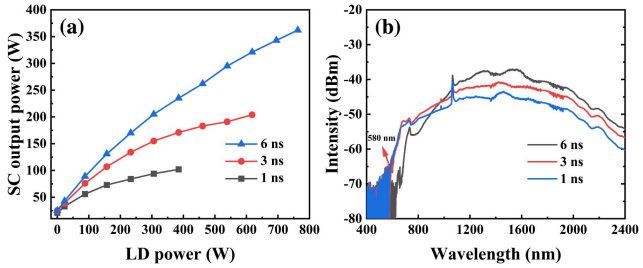

Fig. 6. The dependence of the SC output characteristics on the pulse duration of the seed laser. (a) The SC output power and (b) the SC output spectra.

thermal load. Figure 6(a) plots the SC output power versus the LD power under different pulse durations. As seen from Fig. 6(a), stretching the pulse duration is beneficial for SC power scaling. The maximum SC output power is boosted from 102 W to 204 W and 362 W, when varying the pulse duration from 1 ns up to 3 ns and 6 ns, respectively. This is because a long pulse can extract more energy from the pump, resulting in the increase of the main-amplifier output power and then the SC output power[24]. The final SC output spectra of different pulse durations are shown in Fig. 6(b), and the corresponding pump peak power for 1 ns, 3 ns, and 6 ns is estimated to be 119 kW, 72 kW, and 47 kW, respectively. The flatness and short wavelength extension of the spectrum get worse with increasing pulse duration, which is caused by the inefficient accumulation of soliton-related effects and GPI effects in a lower pump peak power. Both the short wavelength edges of the spectra reach 580 nm when the pulse durations of 1 ns and 3 ns are employed.

A hundred-watt level SC source with a spectrum ranging from 580 nm to 2400 nm and an average output power of 204 W is obtained when the pulse duration of 3 ns is used, as shown in Fig. 7. The inset of Fig. 7 shows the near-field beam profiles of the total and filtered SC. Compared with the inset of Fig. 4,

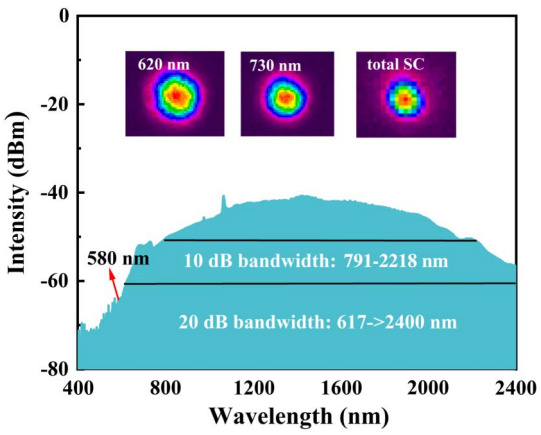

Fig. 7. The final spectrum of the SC at 10 m GRIN MMF with an average output power of 204 W. The repetition rate and pulse duration of the seed laser are fixed at 2 MHz and 3 ns, respectively. The inset shows the near-field beam profiles of the total and filtered SC at different central wavelengths of 730 nm and 620 nm measured at maximum SC output power.

it presents a poor state, resulting from the weaker beam self-cleaning induced by the lower pump peak power[16]. In the experiment of SC power scaling, the improvement of the spectrum characteristics requires the high pump peak power. However, a high pump peak power will cause the nonlinear spectral broadening of the main-amplifier and then prevent further power scaling of the SC. Hence, the best SC output performance needs to effectively balance the relationship between the short wavelength extension of the SC and the SC power scaling.

3. Effect of the GRIN MMF Length on GPI

It can be seen from the above that the GPI effect plays a very important role in the shortwave extension of the SC. Next, we will experimentally demonstrate the influence of the GRIN MMF length on the GPI effect. In general, it is difficult to demonstrate experimentally because other nonlinear effects relating to the fiber length will affect the experimental results. Previous studies had simulated the relationship between the GPI effect and the fiber length on a shorter fiber scale (< 1 m). The results indicate that GPI first generates a series of narrow spectral sidebands, which subsequently broaden upon propagation[13]. However, studies on the influence of the fiber length on the GPI effects still need to be supplemented. In this work, the short wavelength expansion of the SC depends mainly on the GPI effect and the interplay between spatiotemporal soliton oscillations and the DWs. Hence, the influence of the length of the GRIN MMF on the GPI effect can be demonstrated experimentally by contrasting the spectrum region dominated by the GPI effect under different fiber lengths.

Similar to a single mode fiber, a longer fiber length and a higher pump peak power are beneficial to the accumulation of the soliton-related effects in GRIN MMF[25]. The mechanism of the short wavelength extension of the SC caused by the interplay between spatiotemporal soliton oscillations and the DWs is mainly due to the soliton trapping of the DWs[26]. In order to define the short wavelength cut-off edge of the DWs, we calculate the group velocity matching curves of the first three radially symmetric modes, as shown in Fig. 8, where these curves are basically overlapped. When the long wavelengths of the modes reach about 2500 nm, the corresponding short wavelengths with the same group velocity are all about 600 nm.

In the experiments, the GRIN MMFs with three different fiber lengths of 0.5 m, 10 m, and 100 m are employed here to analyze the influence of the GRIN MMF length on the GPI effect. The experiment setup is shown in Fig. 2. The repetition frequency and pulse duration are set at 0.5 MHz and 1 ns. In order to reduce experimental error, we adopt the cut-back measurement method and keep the output coupling position unchanged.

Figure 9 shows the spectral evolution of the SC under three different GRIN MMF lengths for different pump powers. In this section, we focus our attention on the short wavelength region of the spectrum dominated by the GPI effect. The output spectra of the GRIN MMFs with two lengths of 10 m and 100 m are extracted from Figs. 9(c) and 9(d) and are then shown in

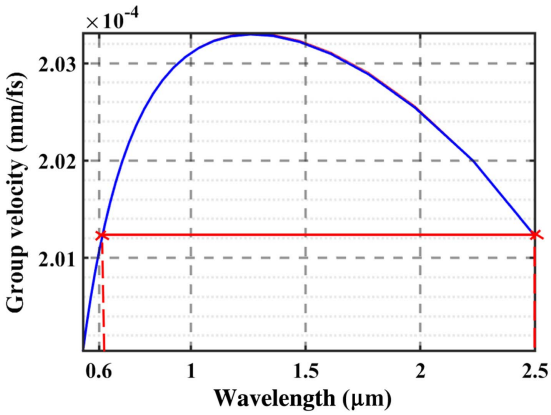

Fig. 8. The group velocity matching curves of the first three radially symmetric modes.

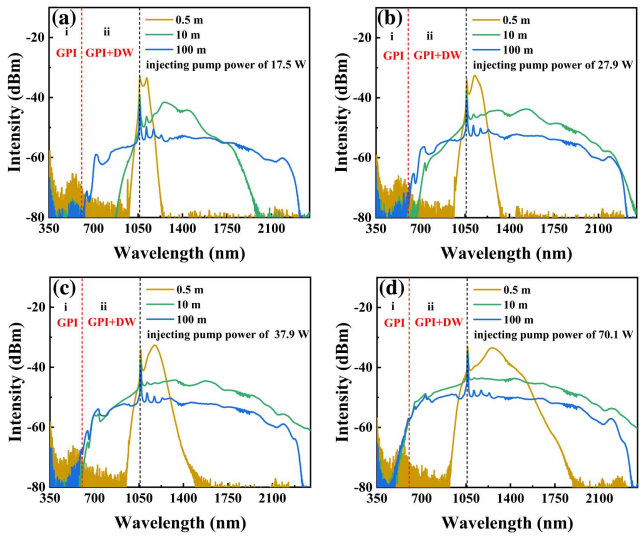

Fig. 9. The spectral evolution of the SC with increasing GRIN MMF lengths under different pump laser powers of (a) 17.5 W, (b) 27.9 W, (c) 37.9 W, and (d) 70.1 W. The red dotted lines represent the cut-off wavelength of the DWs, i.e., 600 nm. Region i is the spectral region dominated by the GPI effect, and region ii is the spectral region dominated by both the DW and the GPI effect. The wavelength peaks in the short wavelength region that appeared in (a)–(d) basically all correspond to the position of GPI peak.

Fig. 10. As seen from Fig. 10(a), under the average pump power of 37.9 W, the spectral short wavelength edges of both GRIN MMF lengths are extended to 600 nm. However, the final short wavelength cut-off edges of the spectra are not reached at this time. When the output pump power further increases to 70.1 W, as shown in Fig. 10(b), the spectral short wavelength edges of both GRIN MMF lengths are extended by 120 nm. The extended part is zoomed-in and shown in the inset of Fig. 10(b). Three wavelength peaks are obviously observed in the inset, corresponding to the wavelength positions of 3rd, 5th, and 6th order GPI peaks, which indicates that the extended part of the spectra is mainly caused by the GPI effect, and the

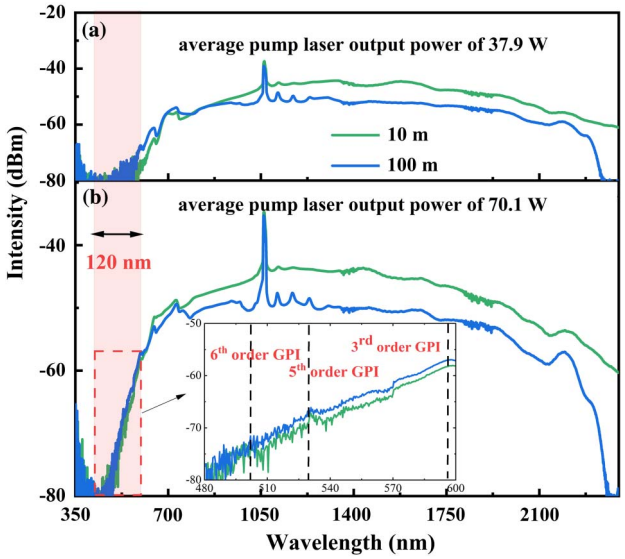

Fig. 10. The spectral evolution of the SC with two kinds of GRIN MMF lengths under different pump laser powers of (a) 37.9 W and (b) 70.1 W. The inset is a zoomed-in view.

final short wavelength extension edges of the spectra are determined by the GPI effect. Note that in the extended part of the spectra induced by GPI, the output spectra of 10 m and 100 m GRIN MMFs are basically overlapped, which indicates that GPI effect is basically independent of the GRIN MMF length on a longer fiber scale.

Based on the analysis mentioned above, we further analyze the combined action of the DW and the GPI in the spectral region of the short wavelength expansion. Under a low pump power, as shown in Fig. 9(a), the short wavelength edge of the spectrum is extended to 600 nm first when the 100 m length of the GRIN MMF is used. During this process of the spectrum evolution along the fiber length, the GRIN MMF length has a great influence on the short wavelength expansion of the spectrum, which indicates that the DW plays a major role in this process. With the increase of the pump power, the short wavelength expansion of the spectrum induced by the DW also basically stops in terms of the 100 m GRIN MMF. Then, the spectral short wavelength edge of 10 m GRIN MMF is accelerated to catch up with that of 100 m GRIN MMF due to the combined action of the DW and the GPI [Figures 9(a)–9(c)]. As shown in Fig. 9(d), further increasing the pump power causes the spectral short wavelength edges of both GRIN MMFs with the lengths of 10 m and 100 m, respectively, to reach 480 nm under the action of the GPI effect. Note that although the final extension to 480 nm is mainly determined by the GPI effect, the DW also plays a driving role during the process of the short wavelength extension. A too small GRIN MMF length is not conducive to the accumulation of the DW and thus cannot provide seed for the GPI gain located in the spectral region of the working DW. As shown in Fig. 9(d), the 1st order GPI peak did not appear even when the pump power reaches 70.1 W at 0.5 m GRIN MMF.

4. Conclusion

In summary, the potential of SC power scaling based on the GRIN MMF is explored, and the influence of the GRIN MMF length on the GPI effect is analyzed. A cost-effective all-fiber SC source with an average power of 40 W and a spectrum ranging from 450 nm to beyond 2400 nm is obtained using a three-stage MOPA configuration. When employing a four-stage MOPA configuration, a 204 W SC with a spectrum ranging from 580 nm to beyond 2400 nm is achieved. Compared to previous work, not only is the SC power markedly boosted but the influence of the GRIN MMF length on the GPI effect is also analyzed in detail. We find that the GPI effect is basically independent of the GRIN MMF length on a longer fiber scale. These results can be used as a supplement for the GPI effect and also provide a solid foundation for the further development of a low-cost, all-fiber, and high-power visible SC source.

Acknowledgement

This work was supported by the Natural Science Foundation of Hunan Province (No. 2022JJ30653).

References

1. T. Hakala, J. Suomalainen, S. Kaasalainen, and Y. Chen, "Full waveform hyperspectral LiDAR for terrestrial laser scanning," Opt. Express **20**, 7119 (2012).
2. L. Hooper, M. Kalita, A. Devine, A. Orec-Archer, and J. Clowes, "White light 50 W supercontinuum: roadmap to kW truly white lasers," Proc. SPIE **9344**, 93440X (2015).
3. J. M. Dudley, G. Genty, and S. Coen, "Supercontinuum generation is photonic crystal fiber," Rev. Mod. Phys. **78**, 1135 (2006).
4. J. C. Knight, "Photonic crystal fibres," Nature **424**, 847 (2003).
5. C. Liu, J. Lü, W. Liu, F. Wang, and P. K. Chu, "Overview of refractive index sensors comprising photonic crystal fibers based on the surface plasmon resonance effect [Invited]," Chin. Opt. Lett. **19**, 102202 (2021).
6. W. J. Wadsworth, N. Joly, J. C. Knight, T. A. Birks, F. Biancalana, and P. St.J. Russell, "Supercontinuum and four-wave mixing with *Q*-switched pulses in endlessly single-mode photonic crystal fibres," Opt. Express **12**, 299 (2004).
7. D. Chung, H. S. Park, F. Rotermund, and B. Y. Kim, "Measurement of bending-induced birefringence in a hollow-core photonic crystal fiber," Opt. Lett. **44**, 5872 (2019).
8. M. F. Saleh and F. Biancalana, "Ultra-broadband supercontinuum generation in gas-filled photonic-crystal fibers: the epsilon-near-zero regime," Opt. Lett. **46**, 1959 (2021).
9. P. Mondal and S. K. Varshney, "Experimental observation of Kerr beam self-cleaning in graded-index multimode fiber from higher-order mode to fundamental mode," Opt. Fiber Technol. **65**, 102587 (2021).
10. Z. Liu, L. G. Wright, D. N. Christodoulides, and F. W. Wise, "Kerr self-cleaning of femtosecond-pulsed beams in graded-index multimode fiber," Opt. Lett. **41**, 3675 (2016).
11. K. Krupa, A. Tonello, B. M. Shalaby, M. Fabert, A. Barthélémy, G. Millot, S. Wabnitz, and V. Couderc, "Spatial beam self-cleaning in multimode fibres," Nat. Photon. **11**, 237 (2017).
12. K. Krupa, C. Louot, V. Couderc, M. Fabert, R. Guenard, B. M. Shalaby, A. Tonello, D. Pagnoux, P. Leproux, and A. Bendahmane, R. Dupiol, G. Millot, and S. Wabnitz, "Spatiotemporal characterization of supercontinuum extending from the visible to the Mid-infrared in multimode graded-index optical fiber," Opt. Lett. **41**, 5785 (2016).
13. K. Krupa, A. Tonello, A. Barthélémy, V. Couderc, B. M. Shalaby, A. Bendahmane, G. Millot, and S. Wabnitz, "Observation of geometric parametric instability induced by the periodic spatial self-imaging of multimode waves," Phys. Rev. Lett. **116**, 183901 (2016).
14. H. Pourbeyram, G. P. Agrawal, and A. Mafi, "Stimulated Raman scattering cascade spanning the wavelength range of 523 to 1750 nm using a graded-index multimode optical fiber," Appl. Phys. Lett. **102**, 201107 (2013).
15. L. G. Wright, S. Wabnitz, D. N. Christodoulides, and F. W. Wise, "Ultrabroadband dispersive radiation by spatiotemporal oscillation of multimode waves," Phys. Rev. Lett. **115**, 223902 (2015).
16. G. Lopez-Galmiche, Z. Sanjabi Eznaveh, M. A. Eftekhar, J. Antonio Lopez, L. G. Wright, F. Wise, D. Christodoulides, and R. Amezcua Correa, "Visible supercontinuum generation in a graded index multimode fiber pumped at 1064 nm," Opt. Lett. **41**, 2553 (2016).
17. T. Zhang, W. Zhang, X. Hu, R. Pan, Z. Wang, H. Wang, and Y. Wang, "All fiber structured supercontinuum source based on graded-index multimode fiber," Laser Phys. Lett. **19**, 035101 (2022).
18. M. H. Frosz, O. Bang, and A. Bjarklev, "Soliton collision and Raman gain regimes in continuous-wave pumped supercontinuum generation," Opt. Express **14**, 9391 (2006).
19. L. Yang, Y. Yang, B. Zhang, X. Zhu, D. Zhao, S. Liu, and J. Hou, "Record power and efficient mid-infrared supercontinuum generation in germania fiber with high stability," High Power Laser Sci. **10**, e36 (2022).
20. Y. Zhu, Z. Zheng, X. Ge, G. Du, S. Ruan, C. Guo, P. Yan, P. Hua, L. Xia, and Q. Lü, "High-power, ultra-broadband supercontinuum source based upon 1/1.5 μm dual-band pumping," Chin. Opt. Lett. **19**, 041403 (2021).
21. X. Ma, J. Xu, J. Ye, Y. Zhang, L. Huang, T. Yao, J. Leng, Z. Pan, and P. Zhou, "Cladding-pumped Raman fiber laser with 0.78% quantum defect enabled by phosphorus-doped fiber," High Power Laser Sci. **10**, e8 (2022).
22. X. Zhu, F. Yu, D. Wu, Y. Feng, S. Chen, Y. Jiang, and L. Hu, "Low-threshold continuous operation of fiber gas Raman laser based on large-core anti-resonant hollow-core fiber," Chin. Opt. Lett. **20**, 071401 (2022).
23. X. Qi, S. Chen, Z. Li, T. Liu, Y. Ou, N. Wang, and J. Hou, "High-power visible-enhanced all-fiber supercontinuum generation in a seven-core photonic crystal fiber pumped at 1016 nm," Opt. Lett. **43**, 1019 (2018).
24. M. Yang, P.-X. Li, D.-S. Wang, K.-X. Yu, X.-Y. Dong, T.-T. Wang, C.-F. Yao, and W.-X. Yang, "All-fiberized very-large-mode-area Yb-doped fiber based high-peak-power narrow-linewidth nanosecond amplifier with tunable pulse width and repetition rate," Chin. Phys. B **29**, 114206 (2020).
25. L. G. Wright, D. N. Christodoulides, and F. W. Wise, "Controllable spatiotemporal nonlinear effects in multimode fibres," Nat. Photon. **9**, 306 (2015).
26. Z. Deng, Y. Chen, J. Liu, C. Zhao, and D. Fan, "Spatio-temporal control of dispersive waves trapping by solitons in graded-index multimode fibers," Appl. Phys. Express **13**, 112003 (2020).